

3D printing of metals in rapid prototyping of biomaterials: Techniques in additive manufacturing

2

S.L. Sing, C.F. Tey, J.H.K. Tan, S. Huang, Wai Yee Yeong
Singapore Centre for 3D Printing (SC3DP), School of Mechanical and Aerospace Engineering, Nanyang Technological University (NTU), Singapore, Singapore

2.1 Introduction

Among the three-dimensional (3D) printing, or officially known as additive manufacturing (AM), techniques, the powder bed fusion (PBF) and directed energy deposition (DED) are most commonly used to process metals directly as they have the capability to produce high-quality parts that are fully dense. According to ISO/ASTM 52900:2017, PBF is a group of AM processes in which thermal energy selectively fuses regions of a powder bed, while DED is another group of AM processes in which focused thermal energy is used to fuse materials by melting as they are being deposited.

In the academia, there has been extensive studies applying 3D printing in tissue engineering (Sudarmadji et al., 2011; Yeong et al., 2009; Wiria et al., 2007; Yang et al., 2002). For example, tissue scaffolds for cardiac and bone have been fabricated successfully (Chua and Yeong, 2014; Yeong et al., 2004). These applications have mainly focused on using polymers; however, in recent years, there has been growing interest in using metallic biomaterials to create implants. This is made possible with the advancement in 3D printing and accelerated development of printable materials.

In this chapter the application of these two groups of AM technologies in fabrication of metallic biomaterials is described, with specific focus on metals that are biocompatible and commonly used such as 316L stainless steel, titanium-6aluminum-4vanadium (Ti6Al4V), and cobalt-chromium-molybdenum (CoCrMo).

2.2 3D printing techniques for metallic biomaterials

2.2.1 Powder bed fusion

PBF processes melt and fuse selective regions of powder according to computer-aided design (CAD) data using an energy source. Current commercially available systems

use laser (for L-PBF) or electron beam (for E-PBF) as energy source. The general steps of the PBF processes are as follows:

- Selective melting of one powder layer (usually 20–100 μm for L-PBF and 100 μm for E-PBF in thickness).
- The build platform is lowered by the predetermined powder layer thickness.
- Deposition of a next layer of powder onto the build platform.
- The process is repeated with successive powder layers until the required part is built completely (Chua and Leong, 2014).

There are no sacrificial binders involved in the PBF processes, which allow them to form near-full density parts. This gives them a critical advantage over binder jetting processes in direct metallic part manufacturing. An overview of key steps within PBF is shown in Fig. 2.1.

L-PBF, also commercially known as selective laser melting (SLM) and direct metal laser melting (DMLM), uses a fiber laser as the energy source (Rafi et al., 2013). The whole process is carried out in an inert gas (typically argon or nitrogen)–filled chamber, which ensures higher purity in the fabricated metallic parts. The inert environment minimizes the oxygen in the environment and reduces the risk of hydrogen pickup. The representative schematic of the L-PBF system is shown in Fig. 2.2.

The fiber laser in the L-PBF system can operate up to 1 kW with various spot diameter, depending on the laser module installed in the system (Chua and Leong, 2014). The galvanometer and F-theta lens control the beam focus and the movement of the beam along the build platform, respectively. As mentioned a powder layer of 20–100 μm thickness is spread over the build platform during the process. The powder is carried and spread by the powder recoater across the build platform. Preheating of up to 400°C can be applied on the build platform for some commercial L-PBF systems (Mertens et al., 2018). The laser is then used to selectively melt the sections of the powder layer based on the geometry defined by the CAD file. In most L-PBF systems, every layer of a part is melted in two steps:

1. Contouring—outer boundary of the part is irradiated by the laser and built first
2. The powder within the contour/perimeter is melted subsequently

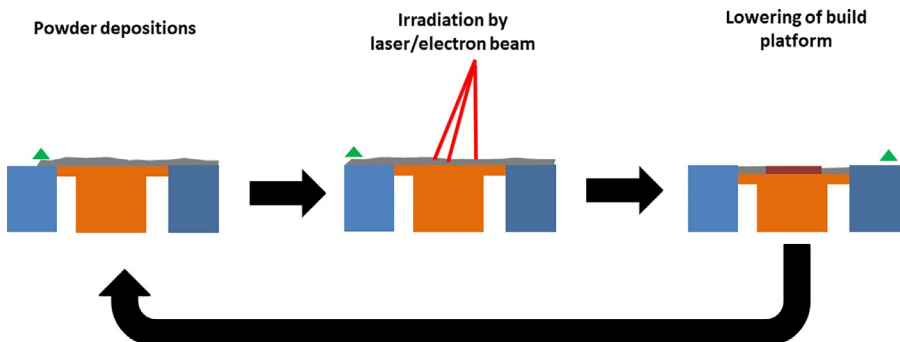


Fig. 2.1 Schematic of PBF.

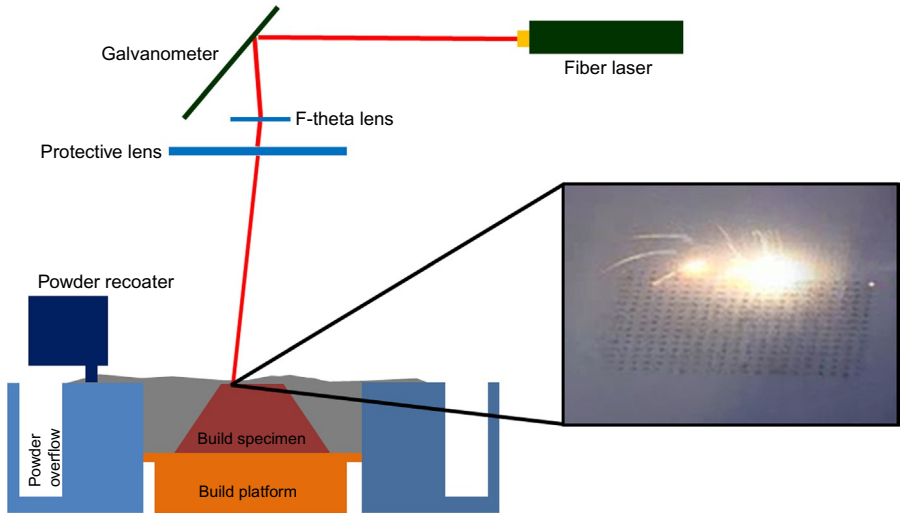


Fig. 2.2 Schematic of L-PBF, also known as selective laser melting (Sing et al., 2016a).

After the two steps of the melting process, another powder layer is then deposited. This process continues until the desired 3D part is fully completed (Thijs et al., 2010). L-PBF has been utilized to fabricate orthopedic implants such as replacements for zygomatic bone (Rotaru et al., 2015) and finger (Merkel et al., 2014).

E-PBF, also commercially known as electron beam melting (EBM), is another metal 3D printing technique. As the name suggests, electron beam energy is used to melt the metal powder during the process (Parthasarathy et al., 2010). The entire process has to take place in a vacuum chamber due to the usage of electron beam as the energy source. The vacuum chamber provides additional advantages such as high part purity due to the oxygen-free environment and reduction in hydrogen pickup. This is critical for fabricating parts out of highly reactive biomaterials such as Ti6Al4V as the low levels of interstitial elements need to be controlled during fabrication. Furthermore, E-PBF-produced parts have lower residual stresses, and hence, warpage and distortion as the chamber is maintained at an elevated temperature of about 700°C during the process. A schematic of E-PBF system is shown in Fig. 2.3.

The electron gun in the E-PBF system operates at a 60kW to generate a focused energy beam density that is above 100kW/cm². The electromagnetic lenses and the deflection coils control the beam focus and the movement of the beam along the build platform, respectively. A powder layer of 100µm thickness is spread across the build platform during the process by the moving rake. The moving rake brings powder from both hoppers inside at the build chamber (one at each side). Preheating of the powder layer is achieved using the electron beam with a higher scan speed for every layer. This is followed by the actual melting of the powder layer based on the geometry defined by the CAD file. Like the L-PBF, every layer of a part is built in two steps, contouring and the melting of the remaining cross section. This process continues until the desired

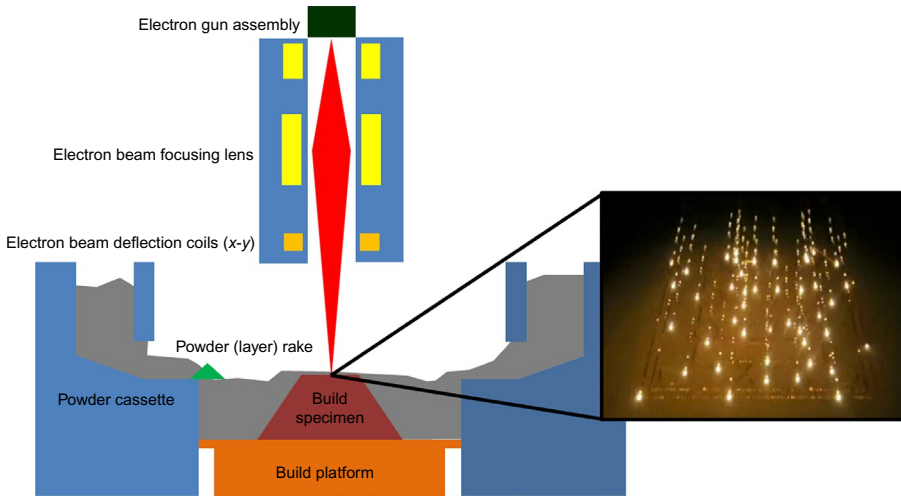


Fig. 2.3 Schematic of E-PBF, also commonly known as electron beam melting (Sing et al., 2016a).

3D part is fully completed (Rafi et al., 2013). Due to well-controlled environment, E-PBF has been used to produce orthopedic components such as maxillofacial plates, hip, knee, and jaw replacements (Cronskar et al., 2013; Mazzoli et al., 2009; Jardini et al., 2014a,b).

2.2.2 Directed energy deposition

DED is a group of AM processes that adds material alongside the heat input simultaneously. The heat input can either be a laser, electron beam, or plasma arc. The material feedstock is either metal powder or wire. Powders result in lower deposition efficiency compared with metal wires as only a part of the total powder would be melted and bonded to the substrate (Lee, 2008). Like the E-PBF, electron beam systems in DED require vacuum and would not have high oxidation issues and laser system and, on the other hand, require other methods to introduce inert gases. Powder DED machines often have inert gas blown together with the powder from the nozzles, thereby sheathing the melted region, reducing the oxidation rate (Gokuldoss et al., 2017). Powder DED systems can use single or multiple nozzles to eject the metal powders (Mazzucato et al., 2017). Using multiple nozzles allows the possibility of mixing different materials to get functionally graded materials (FGM) (Liu and DuPont, 2003; Li et al., 2017). A schematic of the DED systems are shown in Fig. 2.4.

DED systems can differ from PBF systems as powders used are often larger in size and require higher energy density (Yusuf and Gao, 2017; Lewandowski and Seifi, 2016). This results in faster build rates as compared with PBF system. However, this leads to poorer surface quality that may require additional machining. Support structures commonly used in PBF systems is seldom or never used in DED that often

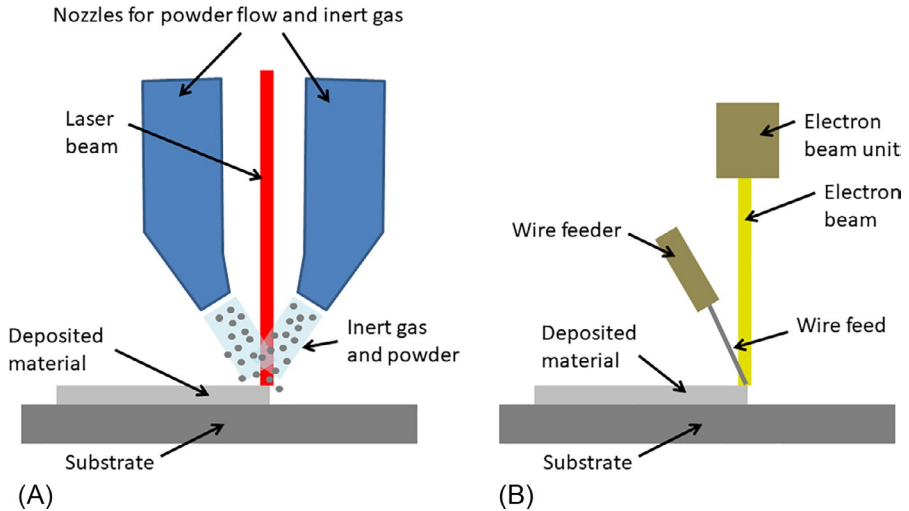


Fig. 2.4 Schematics of two DED systems (A) uses laser together with powder feedstock and (B) uses electron beam and wire feedstock.

uses multiple axis turntables to rotate the build platform to achieve the varying features. Without the need for a powder bed, DED systems can do repair or printing on existing parts.

2.3 3D printed metallic biomaterials

2.3.1 316L stainless steel

316L stainless steel is a common choice for biomaterial, due to its good biocompatibility, availability, and low cost. As a result, it is well suited for use in prostheses and implants when coupled with 3D printing for individualized and customized parts at low costs.

The building accuracy and part quality such as density of orthodontic products using 316L stainless steel are investigated by Yang et al. using a self-developed L-PBF machine. The required surface quality and mechanical properties are achieved in their study (Yang et al., 2012). Structures with gradient porosity are fabricated and studied by Li et al. using L-PBF 316L stainless steel. The dense portion is designed for strength, while the porous portion is designed to enhance tissue growth in biocompatible implants (Li et al., 2010). Using 316L stainless steel and L-PBF, Bibb et al. (2006) fabricated denture framework. The same research group also presented four case studies using L-PBF 316L stainless steel surgical guides in different maxillo-facial (jaw and face) surgeries (Bibb et al., 2009). Kruth et al. (2005a) developed a biocompatible metal framework for dental prostheses, and Wehmoller et al. (2005) reported body implants of cortical bone, mandibular canal segment, and support structures or tubular bone made from L-PBF 316L stainless steel. In comparison,

medical applications using 316L stainless steel processed by E-PBF and DED are limited at the time of writing.

2.3.1.1 Relative density

The relative density of a part is often used as an indicator of the quality of the 3D printed metallic parts. Relative density is the ratio of the density of the 3D printed part to the theoretical density of the bulk material. Using L-PBF, [Tolosa et al. \(2010\)](#) were able to obtain a relative density of 99.90%, and [Yasa et al. \(2011\)](#) obtained a better relative density of 99.95% with laser remelting. However, laser remelting increases the energy used and production time as each layer is scanned twice. With E-PBF, [Wang et al. \(2018\)](#) were able to achieve a relative density of more than 98.8%, while [Zhong et al. \(2017\)](#) recorded a relative density of 99.8% using the same process. [Tan et al. \(2019\)](#) reported a relative density of more than 99.8% for 316L stainless steel parts produced by DED.

2.3.1.2 Mechanical properties

Due to its superior mechanical strength, 316L stainless steel has numerous applications. It is of interest to note that the different microstructures resulted from each AM process lead to different properties. Due to rapid cooling in L-PBF process, the microstructure obtained is more refined, which results in higher tensile strength but with a reduction in ductility compared with forged counterparts. The mechanical properties of 316L stainless steel parts produced by 3D printing and forging are shown in [Table 2.1](#).

Table 2.1 Mechanical properties of 316L stainless steel by L-PBF, E-PBF, DED, and forging.

Properties	L-PBF	E-PBF	DED	Forging
Ultimate tensile strength (MPa)	480–760 (Spierings et al., 2011 ; Kruth et al., 2005b ; Liu et al. 2014)	437–580 (Wang et al., 2018 ; Zhong et al., 2017)	533–685 (Wang et al., 2019 ; Yadollahi et al., 2015)	450–818 (Zhang and Wang, 2014 ; Venugopal et al., 1996)
Yield strength (MPa)	350–640 (Spierings et al., 2011, 2013)	253–396 (Wang et al., 2018 ; Zhong et al., 2017)	235–485 (Wang et al., 2019 ; Yadollahi et al., 2015)	150–230 (Zhang and Wang, 2014 ; Kong et al., 2009)
Elongation (%)	10–30 (Kruth et al., 2005b ; Spierings et al., 2013)	10–59 (Wang et al., 2018 ; Zhong et al., 2017)	12–43 (Yadollahi et al., 2015)	50–62 (Zhang and Wang, 2014 ; Venugopal et al., 1996)
Microhardness (HV)	220–279 (Kruth et al., 2005b ; Liu et al., 2014)	165–173 (Zhong et al., 2017 ; Rannar et al., 2017)	182–210 (Tan et al., 2019 ; Kim et al., 2019)	133–140 (Zhang and Wang, 2014)

2.3.2 Titanium-6aluminum-4vanadium

3D printing of Ti6Al4V has gained much interest in the past decade due to its various applications, especially in biomedical industries. The high strength-to-weight ratio, biocompatibility, and corrosion resistance make it suitable for many lightweight applications such as orthopedic implants (Murr et al., 2010). In comparison with stainless steels and CoCrMo alloys, Ti6Al4V features a lower elastic modulus that is closer to those of the bone, making it slightly more favorable for minimizing the stress shielding effect.

Several groups have research on the mechanical properties and compatibility of additively manufactured Ti6Al4V as body implants. The works of Murr et al. highlight the microstructural features of AM Ti6Al4V (Murr et al., 2009a,b) and the tailorable properties of AM porous meshes (Murr et al., 2010). Warnke et al. (2008) and Hollander et al. (2006) showed that the Ti6Al4V scaffolds produced by L-PBF are biocompatible and support the growth of osteoblasts (bone cells). Van Bael et al. studied the effects of pore geometry on the behavior of human periosteum-derived cells. Based on their in vitro results, it was suggested that a functionally graded scaffold containing small interior pores for initial cell attachment and large exterior pores to avoid cell occlusion may improve the overall scaffold quality (Van Bael et al., 2012). Pattanayak et al. (2011) found that the bone affinity of porous titanium structures fabricated by L-PBF could be improved through chemical and heat treatment. Taniguchi et al. (2016) and Pattanayak et al. (2011) investigated the effects of pore sizes on the bone fixation ability and osteoinduction of porous titanium implants, respectively, and found that a pore size of 0.5–0.6 mm was ideal for both purposes. Furthermore, in vivo tests conducted by Van der Stok et al. (2012) using a rat model also showed that bone formation is facilitated by the titanium scaffolds. A similar conclusion is also drawn from the works of Biemond et al. (2013) who studied the bone ingrowth of trabecular-like surfaces implanted into goats. In addition, Wu et al. (2013a) found that the sheep cervical implants made from porous Ti6Al4V cages demonstrated better osseointegration and mechanical stability as compared with the conventional poly-ether-ether-ketone cage. Evidently, Ti6Al4V and other Ti-based alloys have important applications as biomaterials, and this is further complemented by the design capabilities of 3D printing processes.

2.3.2.1 Relative density

The densities of Ti6Al4V component additive manufactured via L-PBF, E-PBF, and DED are generally very high. The highest relative density reported using L-PBF and DED is 99.80% (Vandenbroucke and Kruth, 2007) and 99.999% (Carroll et al., 2015), respectively. On the other hand, E-PBF-produced part has reported relative density of 99.4% by Facchini et al. (2009).

2.3.2.2 Mechanical properties

Generally the strength of L-PBF-produced Ti6Al4V parts is higher than those produced by E-PBF, but the elongation is lower. This trade-off between strength and ductility may be attributed to the presence of α' phase and the higher residual

stresses induced in the L-PBF process. On the other hand the strength and ductility of the DED parts are comparable with those produced by PBF, respectively.

Under each processing method and operating condition, there may also be part property variation within the component along the build direction. The repeated addition of material causes the underlying build layers to experience numerous cycles of heating and cooling. Consequently the annealing effect is different for each build layer. Additionally the bottom layers also tend to experience a higher cooling rate due to its proximity to the build substrate. The accumulation of these factors leads to a graded microstructure with slight variations in properties from the bottom to the top of the built (Carroll et al., 2015; Tan et al., 2015). The ultimate tensile strength, yield strength, elongation, and microhardness of Ti6Al4V parts produced by 3D printing and casting are shown in Table 2.2.

2.3.3 Cobalt-chromium-molybdenum

CoCrMo has been studied by various groups as biomaterial using 3D printing. Using L-PBF, Oyague et al. and Kim et al. separately evaluated the fit of dental prostheses. However, they reached different conclusions about the suitability of the technology for producing dental prostheses (Kim et al., 2013; Oyague et al., 2012). In terms of hardness, elastic modulus, and strength, Ayyildiz et al. (2013) concluded that CoCrMo produced by laser AM is suitable for dental applications.

Table 2.2 Mechanical properties of L-PBF, E-PBF, DED, and cast Ti6Al4V.

Properties	L-PBF	E-PBF	DED	Cast
Ultimate tensile strength (MPa)	973–1407 (Kasperovich and Hausmann, 2015; Murr et al., 2009c)	915–1200 (Murr et al., 2009a; Facchini et al., 2009)	920–1163 (Qiu et al., 2015; Dinda et al., 2008)	934–1173 (Wei et al., 2011; Ho, 2008)
Yield strength (MPa)	885–1333 (Kasperovich and Hausmann, 2015; Murr et al., 2009c)	830–1150 (Murr et al., 2009a; Facchini et al., 2009)	850–1105 (Qiu et al., 2015; Dinda et al., 2008)	862–999 (Wei et al., 2011; Ho, 2008)
Elongation (%)	5–19 (Kasperovich and Hausmann, 2015; Murr et al., 2009c)	13–25 (Murr et al., 2009a; Facchini et al., 2009)	4–17 (Qiu et al., 2015; Dinda et al., 2008)	6–7 (Wei et al., 2011; Ho, 2008)
Hardness (HV)	381–479 (Thijs et al., 2010)	360–460 (Murr et al., 2009a)		294–360 (Ho et al., 1999; Jovanovic et al., 2006)

2.3.3.1 Relative density

For L-PBF, a relative density of 99.94% by L-PBF is achieved for CoCrMo (Sanz and Navas, 2013). Tan et al. (2018) obtained a relative density of higher than 99.2% from CoCrMo by E-PBF. España et al. (2010) reported relative density of up to 88% for DED produced CoCrMo parts.

2.3.3.2 Mechanical properties

CoCrMo has uses in implants, but the mechanical properties of CoCrMo produced by DED have little literature. Table 2.3 shows the mechanical properties for CoCrMo using 3D printing techniques and casting.

2.4 Challenges, potential and current active research in 3D printing of metallic biomaterials

2.4.1 New material systems

Biodegradable metal implants can be useful in providing temporarily mechanical support during the healing process of injured or pathological tissue (Witte et al., 2008). The selection of materials to fulfill this purpose is highly dependent on the

Table 2.3 Mechanical properties of L-PBF, E-PBF, DED, and cast CoCrMo.

Properties	L-PBF	E-PBF	DED	Casting
Ultimate tensile strength (MPa)	951–1308 (Takachi et al., 2013; Aveyanova et al., 2011; Wu et al., 2013b)	1450 (Gaytan et al., 2010)		591–759 (Takachi et al., 2013; Aveyanova et al., 2011)
Yield strength (MPa)	562–884 (Takachi et al., 2013; Aveyanova et al., 2011; Wu et al., 2013b)	510 (Gaytan et al., 2010)		296–568 (Takachi et al., 2013; Aveyanova et al., 2011)
Elongation (%)	10–16 (Takachi et al., 2013; Aveyanova et al., 2011; Wu et al., 2013b)	3.6 (Tolosa et al., 2010)		8.0–10.7 (Takachi et al., 2013; Aveyanova et al., 2011)
Microhardness (HV)	458–482 (Ayyildiz et al., 2013; Xin et al., 2013)		380–495 (Mantrala et al., 2015)	324.0–384.8 (Xin et al., 2013; Henriques et al., 2012)

mechanical strength, degradation rate, and biocompatibility of the material. As they have similar mechanical properties to natural bones, bioresorbable and noninflammable, magnesium and its alloys have great potential as biomaterials. Furthermore, they are also osteoconductive that encourage cell attachment and bone growth (Alvarez and Nakajima, 2009). Man's group studied the fabrication of lightweight biodegradable and bioresorbable orthopedic implants using L-PBF of magnesium (Zhang et al., 2011; Ng et al., 2011; Ponader et al., 2010). While magnesium has been explored as a suitable candidate as biomaterial, it has the issue of very high degradation rate (Witte et al., 2008). In contrast, iron has the issue of having a low degradation rate (Hermawan et al., 2010). Zinc has been a recently emerging material for biodegradable implant due to its intermediate degradation rate between magnesium and iron (Demir et al., 2017). Due to this, there is a recent surge in publications on the L-PBF of zinc as a biodegradable material (Demir et al., 2017; Wen et al., 2018a,b; Marco et al., 2017). In addition, Shuai et al. (2017) has even attempted to further modify the mechanical properties and degradation behavior of L-PBF-produced zinc with the addition of silver.

As discussed in previous sections, Ti6Al4V has been widely used as biomaterial, but the cytotoxicity of its constituent elements certainly raises concerns. The high cytotoxicity of vanadium has been shown (Ghosh et al., 2015), and the potential of aluminum to cause the Alzheimer disease has been discussed (Perl and Brody, 1980). Recent focus has been on the AM of implants using titanium alloys that can consist of nontoxic elements such as niobium, tantalum, zirconium, and tin. In addition, the alloys' composition is usually adjusted such that they are beta or near beta stabilized, giving low elastic modulus that reduces the stress shielding effect. Ti-24Nb-4Zr-8Sn (Ti2448) has been examined with L-PBF (Liu et al., 2015, 2016a) and E-PBF (Liu et al., 2016a,b, 2017) as a material with high strength-to-elastic modulus ratio. Moreover, Ti-xNb alloy has been manufactured using L-PBF (Weinmann et al., 2018; Sharkeev et al., 2017; Fischer et al., 2016; Schulze et al., 2018) and DED (Fischer et al., 2017) processes. Meanwhile the Ti-xNb-yZr (Zhou et al., 2018a,b; Kreitzberg et al., 2018) and Ti-37Nb-6Sn (Chen et al., 2018) have also been explored with the L-PBF process.

Furthermore, composite materials were studied to modify properties of titanium implants such as biocompatibility and wear resistance. Han et al. (2017) demonstrated the fabrication of titanium/nanohydroxyapatite composites with L-PBF to improve the bioactivity and wear resistance of pure titanium implant but with tensile strength significantly decreased. Functionally graded titanium/hydroxyapatite composites have also been studied and successfully improved the hardness of titanium matrix while sacrificing the fracture toughness (Han et al., 2018). The improvement of hardness and wear resistance were also done by the addition of TiB (Attar et al., 2017) and TiB+TiC (Xia et al., 2017) into titanium matrix.

The development of new materials in AM first requires sufficient process parameter optimization to reduce the amount of porosity, which can be done experimentally with the guidance of process simulation. With attempts to monitor the melt pool behavior in L-PBF process (Leung et al., 2018; Zhao et al., 2017), the porosity formation of parts built via L-PBF can be better understood. This will potentially improve the accuracy of process simulation and speed up the process parameter optimization.

Regardless, not all alloy compositions will have their prealloyed feedstock suitable for 3D printing. One usual solution for this challenge is to build a part via in situ alloying of elemental powder blend (Fischer et al., 2016; Chen et al., 2018; Sing et al., 2016b, 2018a). If the elements in the powder blend have drastically different melting and boiling point, further complications to the process parameter optimization will occur. A process window is needed to minimize the amount of unmelted particles of refractory element and to minimize the vaporization of element with low boiling point. A process simulation of 3D printing process on elemental powder blend can be useful in detecting this process window but will certainly pose a challenge due to its multimaterial nature.

2.4.2 Porous lattice structures

As free-form fabrication techniques, 3D printing has the capability to fabricate lattice structures that have designed porosity that can be controlled. Porous cellular structures that have comparable compressive strength similar with those of cortical and trabecular bones have been fabricated using 3D printing, with elastic modulus between 0.2 and 6.3 GPa (Cheng et al., 2012). This is crucial for biomaterial as there are critical requirements in designs and porosity levels in biomedical applications. It is, however, of interest to note that there is a need to balance the level of porosity and stability of mechanical performance of the fabricated parts (Habibovic and de Groot, 2007; Tolochko et al., 2002; Lin et al., 2007; Mour et al., 2010). For example, the bone porosity varies radially for long bones. As such the mechanical strength of the bone decreases gradually from the outer to inner regions and thus can be regarded as a functionally graded structure (FGS) (Sudarmadji et al., 2011). Fortunately, 3D printing provides the key advantage in capability to fabricate such FGS (Watari et al., 2004). These parts possess the distinguishing feature of nonhomogeneity with regard to strength-related properties including yield strength, fracture toughness, fatigue, and creep behavior (Kim and Paulino, 2002).

In broad terms, these porous lattice structures can be classified into stochastic or nonstochastic. Stochastic lattice structures have random variations in the designs of the cells. They can differ in shape and size. On the other hand, nonstochastic or periodic lattice structures have one single unit cell design that are repeated in the lattice structures and uniform throughout (Hasib et al., 2015). Despite 3D printing capability to produce complex geometries, there are still many challenges in fabrication of lattice structures due to their stringent requirements. Hence the dimensional accuracy (Cheng et al., 2012; Yan et al., 2014a,b; Sing et al., 2018b), mechanical properties (Cheng et al., 2012; Yan et al., 2014a; Amin Yavari et al., 2015; Wauthle et al., 2015; Murr et al., 2011), and biocompatibility (de Wild et al., 2013; Jonitz-Heincke et al., 2013; Hrabe et al., 2013) of the fabricated porous lattice structures are ongoing research. Studies have also been done on the development of automated algorithm for cellular lattice structures. Samples of cellular lattice structures fabricated using SLM is shown in Fig. 2.5. The samples shown clearly demonstrated the capability of 3D printing in producing porous lattice structures from CAD models in different shapes. However, key challenges have also been

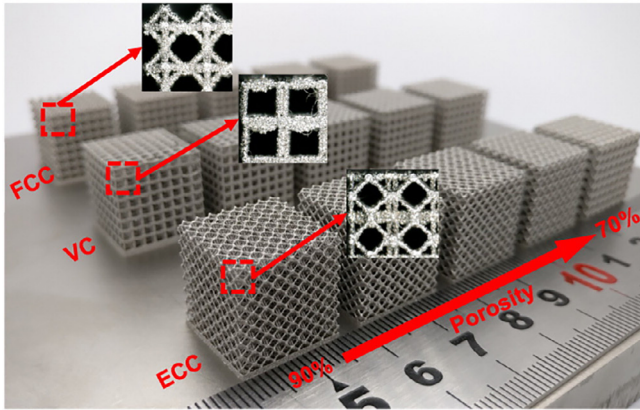


Fig. 2.5 Samples of cellular lattice structures with varying porosities fabricated by L-PBF (Xiao et al., 2018).

identified in additional areas, such as powder adhesions to the struts (Pattanayak et al., 2011) and the difficulty in removal of the unmelted powder within the structures (Hasib et al., 2015).

As mentioned, structures that have varying designs or nonuniform porosities can be called FGS (Birman and Byrd, 2007; Anthoine, 2010). Due to the spatial control of designs and porosity, they are capable to reduce bone remodeling due to the mismatch in mechanical properties, also known as “stress shielding,” between the natural bones and the structures when implanted. This leads to increased biocompatibility with the bone tissues and hence maintaining the bone health (Lin et al., 2009). 3D printing has been proven to be capable of producing very complex geometries with a porosity gradient that varies radially from the center axis of the implant (Traini et al., 2008; Muller et al., 2013). Hence the choice of property distribution in a part can be designed to achieve specific requirements. Samples of FGS fabricated using L-PBF are shown in Fig. 2.6. The fabricated sample has shown the versatility of 3D printing in producing FGS with wide range of porosities.

FGS using titanium and hydroxyapatite have been fabricated by Watari et al. (1996, 2004). Gradient porosities improve both biochemical affinity to osteogenesis and biocompatibility as FGS can be used to control the tissue response (Watari et al., 2004). The design of dental implants using FGS has been investigated by Lin et al. (2009).

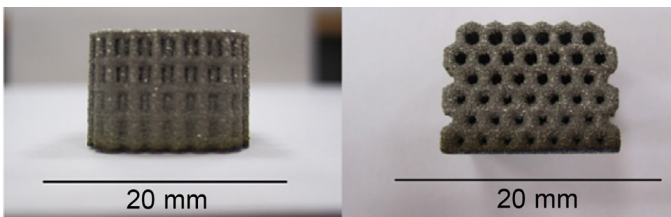


Fig. 2.6 Samples of FGS fabricated by L-PBF (Choy et al., 2017).

It is observed that better performance in bone turnover is achieved with lower FGS gradient; however, there is a higher risk of damage in the early stage of healing as this would reduce the implant stiffness (Lin et al., 2009).

2.4.3 *Multimaterials*

Most biomedical applications currently use parts that are composed of a single material, sometimes with a coating layer, which is essentially uniform in composition and structure in the longitudinal direction (Watari et al., 2004; Muller et al., 2013). This leads to constant properties, such as strength and biocompatibility throughout them. However, a single composition with uniform structure cannot satisfy all the requirements needed for numerous applications (Watari et al., 1996). The properties offered by each biomaterial are unique and have a different set of advantages and limitations. Stainless steel has relatively low cost but has inferior corrosion resistance compared with titanium-based and CoCrMo alloys. Titanium-based alloys have an excellent strength-to-weight ratio and a large range of tailorable elastic modulus but have a relatively low wear resistance. CoCrMo offers exception corrosion and wear resistance but has an unfavorably high elastic modulus of ~ 220 GPa, which may lead to stress shielding. Evidently, no single alloy could be excellent in every requirement. However, a combination of multiple materials may be able to make up for the shortcomings of each alloy. For instance, a combination of Ti6Al4V with CoCrMo may result in a part that possesses both lightweight properties and a superior corrosion and wear resistance. While the potential of multimaterial parts is indeed appealing, there are also challenges associated with the manufacturing of such components. Specifically the dissimilar material interface may contain substantial amounts of intermetallic compounds, which embrittle the interface and reduce the bond strength. An indication of the possible intermetallic compounds that could form between different material combinations can be obtained from the binary or multicomponent phase diagrams. For example, the combination of steel and titanium-based alloys results in the formation of interfacial Fe-Ti intermetallic compounds (Reichardt et al., 2016; Sahasrabudhe et al., 2015; Bobbio et al., 2017), and the combination of titanium to cobalt produces Ti-Co intermetallic compounds (Xue and Wang, 2005; Weng et al., 2014). While these intermetallic compounds generally feature high hardness values and may be beneficial in improving wear resistance (Xue and Wang, 2005; Dutta Majumdar et al., 2009a), their corrosion resistance and biocompatibility requires further investigation. Even though most material combinations yield brittle reaction products, combinations where reaction phases are either absent or suppressed also exist. Some of these compatible material combinations include cobalt and iron, cobalt and nickel, iron and chromium, iron and nickel, nickel and copper, copper and niobium, titanium and tantalum, and titanium and niobium (Sun and Ion, 1995). The compatibility between cobalt and iron indicates that the wear resistance of stainless steel may be improved through a combination with CoCrMo alloy. However, such a combination presents little advantage over the use of a part made entirely from CoCrMo for biomedical applications because the specific strength, corrosion resistance, and stress shielding effect of stainless steel are either comparable or inferior

with those of CoCrMo. A common approach used to bond incompatible metallic combination is to introduce intermediate material/s between the terminal alloys such that a direct bonding between the incompatible pair is avoided. For instance, the formation of intermetallic compound can be completely averted by replacing the direct steel/titanium bond with a steel/nickel/copper/niobium/titanium bond (Li et al., 2012) or with a FGM (Reichardt et al., 2016; Bobbio et al., 2017; Hofmann et al., 2014a,b; Tammam-Williams and Todd, 2017; Carroll et al., 2016). FGM are composite materials formed from two or more constituent phases with a continuously variable compositions (Birman and Byrd, 2007; Anthoine, 2010). In addition, FGM has the potential to eliminate the problems arising from mismatch in mechanical properties. FGM signifies a new class of composites, which consists of a graded pattern of material compositions and microstructures or allows better matching of corresponding mechanical properties (Lin et al., 2009; Wang et al., 2002). The resulting FGM can have a microstructure that produces continuous or discrete change in mechanical properties (Aboudia et al., 1999) due to variation in composition (Muller et al., 2013) to allow better functionality as biomaterial.

At present, most of the multimaterial AM research has been conducted using the DED technique due to the relative ease of changing powder compositions in real time (Liu and DuPont, 2003; Reichardt et al., 2016; Sahasrabudhe et al., 2015; Hofmann et al., 2014a,b; Tammam-Williams and Todd, 2017; Carroll et al., 2016; Dutta Majumdar et al., 2009b; Pei et al., 2003; Vamsi Krishna et al., 2008; Balla et al., 2009). Hofmann et al. (2014b) demonstrated that a continuous variation of material composition can be used to produce a functional gradient between the terminal alloys such that a gradual transition of properties is obtained. If two different powder compositions are used in the DED process, the composition gradient may only vary linearly between the terminal compositions. However, if three or more powders are used in the DED process then the composition path between the terminal alloys may follow any arbitrary route on the multicomponent phase diagram to avoid the formation of brittle phases (Hofmann et al., 2014b). In comparison, such flexibilities are not readily available in the PBF processes. Nevertheless, PBF is also capable of producing multimaterial parts using modified powder deposition mechanisms, which are not commercially available at present. Such a mechanism may either consist of a recoater housing that is partitioned to hold different powders (Liu et al., 2014; Sing et al., 2015) or comprise a series of powder containing nozzles mounted on a frame (Al-Jamal et al., 2008; Yang and Evans, 2004). Notably the integration of the latter powder dispensing mechanism with a conventional L-PBF system has been reported by Wei et al. recently (Wei et al., 2018). Using their newly developed multimaterial L-PBF technology, Wei et al. were able to introduce material variations within and across build layers without cross contaminating the different powders. In the case of E-PBF, the multimaterial system has yet to be introduced commercially as it remains a controlled process owned by the original equipment manufacturer, Arcam AB. Nonetheless, there has been ongoing research on the computer simulations (Yan et al., 2016), new mechanism (Guo et al., 2015), and actual fabrication (Terrazas et al., 2014) using E-PBF for multimaterials.

2.5 Conclusion

With the advancement in 3D printing, it is now able to fabricate fully functional metallic parts directly. These techniques provide the biomedical field the opportunities to mass customize at a lower cost due to their ability to fabricate parts with complex and intrinsic designs that are specific to individual patients. To summarize, this chapter shows the immense potential of 3D printing in becoming the more preferred method for processing metallic biomaterials. With the earlier discussed advantages and potential, exciting research will emerge to take advantage of such technologies in this field to overcome existing challenges.

References

- Aboudia, J., Pinderab, M.-J., Arnold, S.M., 1999. Higher-order theory for functionally graded materials. *Compos. Part B* 30, 777–832.
- Al-Jamal, O.M., Hinduja, S., Li, L., 2008. Characteristics of the bond in Cu–H13 tool steel parts fabricated using SLM. *CIRP Ann.* 57, 239–242.
- Alvarez, K., Nakajima, H., 2009. Metallic scaffolds for bone regeneration. *Materials* 2, 790–832.
- Amin Yavari, S., Ahmadi, S.M., Wauthle, R., Pouran, B., Schrooten, J., Weinans, H., Zadpoor, A.A., 2015. Relationship between unit cell type and porosity and the fatigue behavior of selective laser melted meta-biomaterials. *J. Mech. Behav. Biomed. Mater.* 43, 91–100.
- Anthoine, A., 2010. Second-order homogenisation of functionally graded materials. *Int. J. Solids Struct.* 47, 1477–1489.
- Attar, H., Ehtemam-Haghighi, S., Kent, D., Okulov, I.V., Wendrock, H., Bönisch, M., Volegov, A.S., Calin, M., Eckert, J., Dargusch, M.S., 2017. Nanoindentation and wear properties of Ti and Ti-TiB composite materials produced by selective laser melting. *Mater. Sci. Eng. A* 688, 20–26.
- Averyanova, M., Bertrand, P., Verquin, B., 2011. Manufacture of Co-Cr dental crowns and bridges by selective laser melting technology. *Virtual Phys. Prototyp.* 6, 173–185.
- Ayyildiz, S., Soylu, E.H., Ide, S., Kilic, S., Sipahi, C., Piskin, B., Gokce, H.S., 2013. Annealing of Co-Cr dental alloy: effects on nanostructure and Rockwell hardness. *J. Adv. Prosthodont.* 5, 471–478.
- Balla, V.K., DeVasConCellos, P.D., Xue, W., Bose, S., Bandyopadhyay, A., 2009. Fabrication of compositionally and structurally graded Ti–TiO₂ structures using laser engineered net shaping (LENS). *Acta Biomater.* 5, 1831–1837.
- Bibb, R., Eggbeer, D., Williams, R., 2006. Rapid manufacture of removable partial denture frameworks. *Rapid Prototyp. J.* 12, 95–99.
- Bibb, R., Eggbeer, D., Evans, P., Bocca, A., Sugar, A., 2009. Rapid manufacture of custom-fitting surgical guides. *Rapid Prototyp. J.* 15, 346–354.
- Biemond, J.E., Hannink, G., Verdonschot, N., Buma, P., 2013. Bone ingrowth potential of electron beam and selective laser melting produced trabecular-like implant surfaces with and without a biomimetic coating. *J. Mater. Sci. Mater. Med.* 24, 745–753.
- Birman, V., Byrd, L.W., 2007. Modeling and analysis of functionally graded materials and structures. *Appl. Mech. Rev.* 60, 195–216.

- Bobbio, L.D., Otis, R.A., Borgonia, J.P., Dillon, R.P., Shapiro, A.A., Liu, Z.-K., Beese, A.M., 2017. Additive manufacturing of a functionally graded material from Ti-6Al-4V to Invar: experimental characterization and thermodynamic calculations. *Acta Mater.* 127, 133–142.
- Carroll, B.E., Palmer, T.A., Beese, A.M., 2015. Anisotropic tensile behavior of Ti-6Al-4V components fabricated with directed energy deposition additive manufacturing. *Acta Mater.* 87, 309–320.
- Carroll, B.E., Otis, R.A., Borgonia, J.P., Suh, J.-o., Dillon, R.P., Shapiro, A.A., Hofmann, D.C., Liu, Z.-K., Beese, A.M., 2016. Functionally graded material of 304L stainless steel and inconel 625 fabricated by directed energy deposition: characterization and thermodynamic modeling. *Acta Mater.* 108, 46–54.
- Chen, W., Chen, C., Zi, X., Cheng, X., Zhang, X., Lin, Y.C., Zhou, K., 2018. Controlling the microstructure and mechanical properties of a metastable β titanium alloy by selective laser melting. *Mater. Sci. Eng. A* 726, 240–250.
- Cheng, X.Y., Li, S.J., Murr, L.E., Zhang, Z.B., Hao, Y.L., Yang, R., Medina, F., Wicker, R.B., 2012. Compression deformation behavior of Ti-6Al-4V alloy with cellular structures fabricated by electron beam melting. *J. Mech. Behav. Biomed. Mater.* 16, 153–162.
- Choy, S.Y., Sun, C.-N., Leong, K.F., Wei, J., 2017. Compressive properties of functionally graded lattice structures manufactured by selective laser melting. *Mater. Des.* 131, 112–120.
- Chua, C.K., Leong, K.F., 2014. *3D Printing and Additive Manufacturing: Principles and Applications*, fourth ed. World Scientific Publishing Co. Pte. Ltd, Singapore.
- Chua, C.K., Yeong, W.Y., 2014. *Bioprinting: Principles and Applications*. World Scientific Publishing Co. Pte. Ltd, Singapore.
- Cronskar, M., Backstrom, M., Rannar, L.-E., 2013. Production of customized hip stem prostheses – a comparison between conventional machining and electron beam melting (EBM). *Rapid Prototyp. J.* 19, 365–372.
- de Wild, M., Schumacher, R., Mayer, K., Schkommodau, E., Thoma, D., Bredell, M., Kruse Gujer, A., Grätz, K.W., Weber, F.E., 2013. Bone regeneration by the osteoconductivity of porous titanium implants manufactured by selective laser melting: a histological and micro computed tomography study in the rabbit. *Tissue Eng. Part A* 19, 2645–2654.
- Demir, A.G., Monguzzi, L., Previtali, B., 2017. Selective laser melting of pure Zn with high density for biodegradable implant manufacturing. *Addit. Manuf.* 15, 20–28.
- Dinda, G.P., Song, L., Mazumder, J., 2008. Fabrication of Ti-6Al-4V scaffolds by direct metal deposition. *Metall. Mater. Trans. A* 39, 2914–2922.
- Dutta Majumdar, J., Manna, I., Kumar, A., Bhargava, P., Nath, A.K., 2009a. Direct laser cladding of Co on Ti-6Al-4V with a compositionally graded interface. *J. Mater. Process. Technol.* 209, 2237–2243.
- Dutta Majumdar, J., Kumar, A., Li, L., 2009b. Direct laser cladding of SiC dispersed AISI 316L stainless steel. *Tribol. Int.* 42, 750–753.
- España, F.A., Balla, V.K., Bose, S., Bandyopadhyay, A., 2010. Design and fabrication of CoCrMo alloy based novel structures for load bearing implants using laser engineered net shaping. *Mater. Sci. Eng. C* 30, 50–57.
- Facchini, L., Magalini, E., Robotti, P., Molinari, A., 2009. Microstructure and mechanical properties of Ti-6Al-4V produced by electron beam melting of pre-alloyed powders. *Rapid Prototyp. J.* 15, 171–178.
- Fischer, M., Joguet, D., Robin, G., Peltier, L., Laheurte, P., 2016. In situ elaboration of a binary Ti-26Nb alloy by selective laser melting of elemental titanium and niobium mixed powders. *Mater. Sci. Eng. C* 62, 852–859.

- Fischer, M., Laheurte, P., Acquier, P., Joguet, D., Peltier, L., Petithory, T., Anselme, K., Mille, P., 2017. Synthesis and characterization of Ti-27.5Nb alloy made by CLAD® additive manufacturing process for biomedical applications. *Mater. Sci. Eng. C* 75, 341–348.
- Gaytan, S.M., Murr, L.E., Martinez, E., Martinez, J.L., Machado, B.I., Ramirez, D.A., Medina, F., Collins, S., Wicker, R.B., 2010. Comparison of microstructures and mechanical properties for solid and mesh cobalt-base alloy prototypes fabricated by electron beam melting. *Metall. Mater. Trans. A* 41, 3216–3227.
- Ghosh, S.K., Saha, R., Saha, B., 2015. Toxicity of inorganic vanadium compounds. *Res. Chem. Intermed.* 41, 4873–4897.
- Gokuldoss, P.K., Kolla, S., Eckert, J., 2017. Additive manufacturing processes: selective laser melting, electron beam melting and binder jetting—selection guidelines. *Materials* 10, 672.
- Guo, C., Ge, W., Lin, F., 2015. Dual-material electron beam selective melting: hardware development and validation studies. *Engineering* 1, 124–130.
- Habibovic, P., de Groot, K., 2007. Osteoinductive biomaterials—properties and relevance in bone repair. *J. Tissue Eng. Regen. Med.* 1, 25–32.
- Han, C., Wang, Q., Song, B., Li, W., Wei, Q., Wen, S., Liu, J., Shi, Y., 2017. Microstructure and property evolutions of titanium/nano-hydroxyapatite composites in-situ prepared by selective laser melting. *J. Mech. Behav. Biomed. Mater.* 71, 85–94.
- Han, C., Li, Y., Wang, Q., Cai, D., Wei, Q., Yang, L., Wen, S., Liu, J., Shi, Y., 2018. Titanium/hydroxyapatite (Ti/HA) gradient materials with quasi-continuous ratios fabricated by SLM: material interface and fracture toughness. *Mater. Des.* 141, 256–266.
- Hasib, H., Harrysson, O.L.A., West, H.A., 2015. Powder removal from Ti-6Al-4V cellular structures fabricated via electron beam melting. *J. Min. Met. Mater. Soc.* 67, 639–646.
- Henriques, B., Soares, D., Silva, F.S., 2012. Microstructure, hardness, corrosion resistance and porcelain shear bond strength comparison between cast and hot pressed CoCrMo alloy for metal–ceramic dental restorations. *J. Mech. Behav. Biomed. Mater.* 12, 83–92.
- Hermawan, H., Purnama, A., Dube, D., Couet, J., Mantovani, D., 2010. Fe–Mn alloys for metallic biodegradable stents: degradation and cell viability studies. *Acta Biomater.* 6, 1852–1860.
- Ho, W.F., 2008. A comparison of tensile properties and corrosion behavior of cast Ti-7.5Mo with c.p. Ti, Ti-15Mo and Ti-6Al-4V alloys. *J. Alloys Compd.* 464, 580–583.
- Ho, W.F., Ju, C.P., Chern Lin, J.H., 1999. Structure and properties of cast binary Ti–Mo alloys. *Biomaterials* 20, 2115–2122.
- Hofmann, D.C., Kolodziejska, J., Roberts, S., Otis, R., Dillon, R.P., Suh, J.-O., Liu, Z.-K., Borgonia, J.-P., 2014a. Compositionally graded metals: a new frontier of additive manufacturing. *J. Mater. Res.* 29, 1899–1910.
- Hofmann, D.C., Roberts, S., Otis, R., Kolodziejska, J., Dillon, R.P., Suh, J.O., Shapiro, A.A., Liu, Z.K., Borgonia, J.P., 2014b. Developing gradient metal alloys through radial deposition additive manufacturing. *Sci. Rep.* 4, 5357.
- Hollander, D.A., von Walter, M., Wirtz, T., Sellei, R., Schmidt-Rohlfing, B., Paar, O., Erli, H.-J., 2006. Structural, mechanical and in vitro characterization of individually structured Ti–6Al–4V produced by direct laser forming. *Biomaterials* 27, 955–963.
- Hrabe, N.W., Heinel, P., Bordia, R.K., Körner, C., Fernandes, R.J., 2013. Maintenance of a bone collagen phenotype by osteoblast-like cells in 3D periodic porous titanium (Ti-6Al-4 V) structures fabricated by selective electron beam melting. *Connect. Tissue Res.* 54, 351–360.
- Jardini, A.L., Larosa, M.A., de Carvalho Zavaglia, C.A., Bernardes, L.F., Lambert, C.S., Kharmandayan, P., Calderoni, D., Filho, R.M., 2014a. Customised titanium implant fabricated in additive manufacturing for craniomaxillofacial surgery. *Virtual Phys. Prototyp.* 9, 115–125.

- Jardini, A.L., Larosaemail, M.A., Filho, R.M., Zavaglia, C.A.d.C., Bernardes, L.F., Lambert, C.S., Calderoni, D.R., Kharmandayan, P., 2014b. Cranial reconstruction: 3D biomodel and custom-built implant created using additive manufacturing. *J. Craniomaxillofac. Surg* 42 (8), 1877–1884.
- Jonitz-Heincke, A., Wieding, J., Schulze, C., Hansmann, D., Bader, R., 2013. Comparative analysis of the oxygen supply and viability of human osteoblasts in three-dimensional titanium scaffolds produced by laser-beam or electron-beam melting. *Materials* 6, 5398–5409.
- Jovanovic, M.T., Tadic, S., Zec, S., Miskovic, Z., Bobic, I., 2006. The effect of annealing temperatures and cooling rates on microstructure and mechanical properties of investment cast Ti-6Al-4V alloy. *Mater. Des.* 27, 192–199.
- Kasperovich, G., Hausmann, J., 2015. Improvement of fatigue resistance and ductility of TiAl6V4 processed by selective laser melting. *J. Mater. Process. Technol.* 220, 202–214.
- Kim, J.-H., Paulino, G.H., 2002. Finite element evaluation of mixed mode stress intensity factors in functionally graded materials. *Int. J. Numer. Methods Eng.* 53, 1903–1935.
- Kim, K.B., Kim, W.C., Kim, H.Y., Kim, J.H., 2013. An evaluation of marginal fit of three-unit fixed dental prostheses fabricated by direct metal laser sintering system. *Dent. Mater.* 29, 91–96.
- Kim, D.-K., Woo, W., Kim, E.-Y., Choi, S.-H., 2019. Microstructure and mechanical characteristics of multi-layered materials composed of 316L stainless steel and ferritic steel produced by direct energy deposition. *J. Alloys Compd.* 774, 896–907.
- Kong, T.F., Chan, L.C., Lee, T.C., 2009. Experimental study of effects of process parameters in forge-welding bimetallic materials: AISI 316L stainless steel and 6063 aluminium alloy. *Strain* 45, 373–379.
- Kreitzberg, A., Brailovski, V., Prokoshkin, S., 2018. New biocompatible near-beta Ti-Zr-Nb alloy processed by laser powder bed fusion: process optimization. *J. Mater. Process. Technol.* 252, 821–829.
- Kruth, J.P., Mercelis, P., Van Vaerenbergh, J., Froyen, L., Rombouts, M., 2005a. Binding mechanisms in selective laser sintering and selective laser melting. *Rapid Prototyp. J.* 11, 26–36.
- Kruth, J.P., Vandenbroucke, B., Van Vaerenbergh, J., Naert, I., 2005b. Digital manufacturing of biocompatible metal frameworks for complex dental prostheses by means of SLS/SLM. In: *Virtual Prototyping and Rapid Manufacturing – Advanced Research in Virtual and Rapid Prototyping*. Taylor & Francis, London, pp. 139–146.
- Lee, H.-K., 2008. Effects of the cladding parameters on the deposition efficiency in pulsed Nd:YAG laser cladding. *J. Mater. Process. Technol.* 202, 321–327.
- Leung, C.L.A., Marussi, S., Atwood, R.C., Towrie, M., Withers, P.J., Lee, P.D., 2018. In situ X-ray imaging of defect and molten pool dynamics in laser additive manufacturing. *Nat. Commun.* 9, 1355.
- Lewandowski, J.J., Seifi, M., 2016. Metal additive manufacturing: a review of mechanical properties. *Annu. Rev. Mater. Res.* 46, 151–186.
- Li, R.D., Liu, J.H., Shi, Y.S., Du, M.Z., Xie, Z., 2010. 316L stainless steel with gradient porosity fabricated by selective laser melting. *J. Mater. Eng. Perform.* 19, 666–671.
- Li, P., Li, J., Xiong, J., Zhang, F., Raza, S.H., 2012. Diffusion bonding titanium to stainless steel using Nb/Cu/Ni multi-interlayer. *Mater. Charact.* 68, 82–87.
- Li, W., Karnati, S., Kriewall, C., Liou, F., Newkirk, J., Taminger, K.M.B., Seufzer, W.J., 2017. Fabrication and characterization of a functionally graded material from Ti-6Al-4V to SS316 by laser metal deposition. *Addit. Manuf.* 14, 95–104.

- Lin, C.Y., Wirtz, T., LaMarca, F., Hollister, S.J., 2007. Structural and mechanical evaluations of a topology optimized titanium interbody fusion cage fabricated by selective laser melting process. *J. Biomed. Mater. Res. A* 83, 272–279.
- Lin, D., Li, Q., Li, W., Zhou, S., Swain, M.V., 2009. Design optimization of functionally graded dental implant for bone remodeling. *Compos. Part B* 40, 668–675.
- Liu, W., DuPont, J.N., 2003. Fabrication of functionally graded TiC/Ti composites by laser engineered net shaping. *Scr. Mater.* 48, 1337–1342.
- Liu, Z.H., Zhang, D.Q., Sing, S.L., Chua, C.K., Loh, L.E., 2014. Interfacial characterization of SLM parts in multi-material processing: metallurgical diffusion between 316L stainless steel and C18400 copper alloy. *Mater. Charact.* 94, 116–125.
- Liu, Y.J., Li, X.P., Zhang, L.C., Sercombe, T.B., 2015. Processing and properties of topologically optimised biomedical Ti–24Nb–4Zr–8Sn scaffolds manufactured by selective laser melting. *Mater. Sci. Eng. A* 642, 268–278.
- Liu, Y.J., Li, S.J., Wang, H.L., Hou, W.T., Hao, Y.L., Yang, R., Sercombe, T.B., Zhang, L.C., 2016a. Microstructure, defects and mechanical behavior of beta-type titanium porous structures manufactured by electron beam melting and selective laser melting. *Acta Mater.* 113, 56–67.
- Liu, Y., Li, S., Hou, W., Wang, S., Hao, Y., Yang, R., Sercombe, T.B., Zhang, L.-C., 2016b. Electron beam melted beta-type Ti–24Nb–4Zr–8Sn porous structures with high strength-to-modulus ratio. *J. Mater. Sci. Technol.* 32, 505–508.
- Liu, Y.J., Wang, H.L., Li, S.J., Wang, S.G., Wang, W.J., Hou, W.T., Hao, Y.L., Yang, R., Zhang, L.C., 2017. Compressive and fatigue behavior of beta-type titanium porous structures fabricated by electron beam melting. *Acta Mater.* 126, 58–66.
- Mantrala, K.M., Das, M., Balla, V.K., Rao, C.S., Rao, V.V.S.K., 2015. Additive manufacturing of Co-Cr-Mo alloy: influence of heat treatment on microstructure, tribological, and electrochemical properties. *Front. Mech. Eng* 1 (1), 1.
- Marco, M., Gökhan, D.A., Ehsan, M., Maurizio, V., Barbara, P., 2017. Processability of pure Zn and pure Fe by SLM for biodegradable metallic implant manufacturing. *Rapid Prototyp. J.* 23, 514–523.
- Mazzoli, A., Germani, M., Raffaelli, R., 2009. Direct fabrication through electron beam melting technology of custom cranial implants designed in a PHANToM-based haptic environment. *Mater. Des.* 30, 3186–3192.
- Mazzucato, F., Tusacciu, S., Lai, M., Biamino, S., Lombardi, M., Valente, A., 2017. Monitoring approach to evaluate the performances of a new deposition nozzle solution for DED systems. *Technologies* 5, 29.
- Merkt, S., Kleyer, A., Hueber, A.J., 2014. The additive manufacture of patient-tailored finger implants. *Laser Tech. J.* 11, 54–56.
- Mertens, R., Dadbakhsh, S., Van Humbeeck, J., Kruth, J.P., 2018. Application of base plate preheating during selective laser melting. *Procedia CIRP* 74, 5–11.
- Mour, M., Das, D., Winkler, T., Hoenig, E., Mielke, G., Morlock, M.M., Schilling, A.F., 2010. Advances in porous biomaterials for dental and orthopaedic applications. *Materials* 3, 2947–2974.
- Muller, P., Mognol, P., Hascoet, J.-Y., 2013. Modeling and control of a direct laser powder deposition process for functionally graded materials (FGM) parts manufacturing. *J. Mater. Process. Technol.* 213, 685–692.
- Murr, L.E., Esquivel, E.V., Quinones, S.A., Gaytan, S.M., Lopez, M.I., Martinez, E.Y., Medina, F., Hernandez, D.H., Martinez, E., Martinez, J.L., Stafford, S.W., Brown, D.K., Hoppe, T., Meyers, W., Lindhe, U., Wicker, R.B., 2009a. Microstructures and mechanical properties of electron beam-rapid manufactured Ti–6Al–4V biomedical prototypes compared to wrought Ti–6Al–4V. *Mater. Charact.* 60, 96–105.

- Murr, L.E., Quinones, S.A., Gaytan, S.M., Lopez, M.I., Rodela, A., Martinez, E.Y., Hernandez, D.H., Martinez, E., Medina, F., Wicker, R.B., 2009b. Microstructure and mechanical behavior of Ti-6Al-4V produced by rapid-layer manufacturing, for biomedical applications. *J. Mech. Behav. Biomed. Mater.* 2, 20–32.
- Murr, L.E., Gaytan, S.M., Medina, F., Lopez, H., Martínez, E., Machado, B.I., Hernandez, D.H., Martinez, L., Lopez, M.I., Wicker, R.B., Bracke, J., 2010. Next-generation biomedical implants using additive manufacturing of complex, cellular and functional mesh arrays. *Philos. Trans. R. Soc. A Math. Phys. Eng. Sci.* 368, 1999.
- Murr, L.E., Amato, K.N., Li, S.J., Tian, Y.X., Cheng, X.Y., Gaytan, S.M., Martinez, E., Shindo, P.W., Medina, F., Wicker, R.B., 2011. Microstructure and mechanical properties of open-cellular biomaterials prototypes for total knee replacement implants fabricated by electron beam melting. *J. Mech. Behav. Biomed. Mater.* 4, 1396–1411.
- Ng, C.C., Savalani, M.M., Lau, M.L., Man, H.C., 2011. Microstructure and mechanical properties of selective laser melted magnesium. *Appl. Surf. Sci.* 257, 7447–7454.
- Oyague, R.C., Sanchez-Turrión, A., Lopez-Lozano, J.F., Montero, J., Albaladejo, A., Suarez-Garcia, M.J., 2012. Evaluation of fit of cement-retained implant-supported 3-unit structures fabricated with direct metal laser sintering and vacuum casting techniques. *Odontology* 100, 249–253.
- Parthasarathy, J., Starly, B., Raman, S., Christensen, A., 2010. Mechanical evaluation of porous titanium (Ti6Al4V) structures with electron beam melting (EBM). *J. Mech. Behav. Biomed. Mater.* 3, 249–259.
- Pattanayak, D.K., Fukuda, A., Matsushita, T., Takemoto, M., Fujibayashi, S., Sasaki, K., Nishida, N., Nakamura, T., Kokubo, T., 2011. Bioactive Ti metal analogous to human cancellous bone: fabrication by selective laser melting and chemical treatments. *Acta Biomater.* 7, 1398–1406.
- Pei, Y.T., Ocelik, V., De Hosson, J.T.M., 2003. Interfacial adhesion of laser clad functionally graded materials. *Mater. Sci. Eng. A* 342, 192–200.
- Perl, D., Brody, A., 1980. Alzheimer's disease: X-ray spectrometric evidence of aluminum accumulation in neurofibrillary tangle-bearing neurons. *Science* 208, 297–299.
- Ponader, S., Von Wilmsow, C., Widenmayer, M., Lutz, R., Heinel, P., Körner, C., Singer, R.F., Nkenke, E., Neukam, F.W., Schlegel, K.A., 2010. In vivo performance of selective electron beam-melted Ti-6Al-4V structures. *J. Biomed. Mater. Res. A* 92, 56–62.
- Qiu, C., Ravi, G.A., Dance, C., Ranson, A., Dilworth, S., Attallah, M.M., 2015. Fabrication of large Ti-6Al-4V structures by direct laser deposition. *J. Alloys Compd.* 629, 351–361.
- Rafi, H.K., Karthik, N.V., Gong, H., Starr, T.L., Stucker, B.E., 2013. Microstructures and mechanical properties of Ti6Al4V parts fabricated by selective laser melting and electron beam melting. *J. Mater. Eng. Perform.* 22, 3872–3883.
- Rannar, L.-E., Koptuyg, A., Olsen, J., Saeidi, K., Shen, Z., 2017. Hierarchical structures of stainless steel 316L manufactured by electron beam melting. *Addit. Manuf.* 17, 106–112.
- Reichardt, A., Dillon, R.P., Borgonia, J.P., Shapiro, A.A., McEnerney, B.W., Momose, T., Hosemann, P., 2016. Development and characterization of Ti-6Al-4V to 304L stainless steel gradient components fabricated with laser deposition additive manufacturing. *Mater. Des.* 104, 404–413.
- Rotaru, H., Schumacher, R., Kim, S.-G., Dinu, C., 2015. Selective laser melted titanium implants: a new technique for the reconstruction of extensive zygomatic complex defects. *Maxillofac. Plast. Reconstr. Surg.* 37 (1), 1.
- Sahasrabudhe, H., Harrison, R., Carpenter, C., Bandyopadhyay, A., 2015. Stainless steel to titanium bimetallic structure using LENS™. *Addit. Manuf.* 5, 1–8.

- Sanz, C., Navas, V.G., 2013. Structural integrity of direct metal laser sintered parts subjected to thermal and finishing treatments. *J. Mater. Process. Technol.* 213, 2126–2136.
- Schulze, C., Weinmann, M., Schweigel, C., Keßler, O., Bader, R., 2018. Mechanical properties of a newly additive manufactured implant material based on Ti-42Nb. *Materials* 11, 124.
- Sharkeev, Y.P., Eroshenko, A.Y., Khimich, M.A., Glukhov, I.A., Kovalevskaya, Z.G., Nikonova, I.V., 2017. Features of the microstructure of Ti–Nb alloy obtained via selective laser melting. *Bull. Russ. Acad. Sci. Phys.* 81, 1343–1347.
- Shuai, C., Zhou, Y., Yang, Y., Feng, P., Liu, L., He, C., Zhao, M., Yang, S., Gao, C., Wu, P., 2017. Biodegradation resistance and bioactivity of hydroxyapatite enhanced Mg-Zn composites via selective laser melting. *Materials* 10, 307.
- Sing, S.L., Lam, L.P., Zhang, D.Q., Liu, Z.H., Chua, C.K., 2015. Interfacial characterization of SLM parts in multi-material processing: intermetallic phase formation between AlSi10Mg and C18400 copper alloy. *Mater. Charact.* 107, 220–227.
- Sing, S.L., An, J., Yeong, W.Y., Wiria, F.E., 2016a. Laser and electron-beam powder-bed additive manufacturing of metallic implants: a review on processes, materials and designs. *J. Orthop. Res.* 34, 369–385.
- Sing, S.L., Yeong, W.Y., Wiria, F.E., 2016b. Selective laser melting of titanium alloy with 50 wt% tantalum: microstructure and mechanical properties. *J. Alloys Compd.* 660, 461–470.
- Sing, S.L., Wiria, F.E., Yeong, W.Y., 2018a. Selective laser melting of titanium alloy with 50 wt% tantalum: effect of laser process parameters on part quality. *Int. J. Refract. Met. Hard Mater.* 77, 120–127.
- Sing, S.L., Wiria, F.E., Yeong, W.Y., 2018b. Selective laser melting of lattice structures: a statistical approach to manufacturability and mechanical behavior. *Robot. Comput. Integr. Manuf.* 49, 170–180.
- Spierings, A.B., Herres, N., Levy, G., 2011. Influence of the particle size distribution on surface quality and mechanical properties in AM steel parts. *Rapid Prototyp. J.* 17, 195–202.
- Spierings, A.B., Starr, T.L., Wegener, K., 2013. Fatigue performance of additive manufactured metallic parts. *Rapid Prototyp. J.* 19, 88–94.
- Sudarmadji, N., Tan, J.Y., Leong, K.F., Chua, C.K., Loh, Y.T., 2011. Investigation of the mechanical properties and porosity relationships in selective laser-sintered polyhedral for functionally graded scaffolds. *Acta Biomater.* 7, 530–537.
- Sun, Z., Ion, J.C., 1995. Laser welding of dissimilar metal combinations. *J. Mater. Sci.* 30, 4205–4214.
- Takachi, A., Suyalatu, Nakamoto, T., Joko, N., Nomura, N., Tsutsumi, Y., Migita, S., Doi, H., Kurosu, S., Chiba, A., Wakabayashi, N., Igarashi, Y., Hanawa, T., 2013. Microstructures and mechanical properties of Co–29Cr–6Mo alloy fabricated by selective laser melting process for dental applications. *J. Mech. Behav. Biomed. Mater.* 21, 67–76.
- Tammas-Williams, S., Todd, I., 2017. Design for additive manufacturing with site-specific properties in metals and alloys. *Scr. Mater.* 135, 105–110.
- Tan, X., Kok, Y., Tan, Y.J., Descoins, M., Mangelinck, D., Tor, S.B., Leong, K.F., Chua, C.K., 2015. Graded microstructure and mechanical properties of additive manufactured Ti–6Al–4V via electron beam melting. *Acta Mater.* 97, 1–16.
- Tan, X.P., Wang, P., Kok, Y., Toh, W.Q., Sun, Z., Nai, S.M.L., Descoin, M., Mangelinck, D., Liu, E., Tor, S.B., 2018. Carbide precipitation characteristics in additive manufacturing of Co-Cr-Mo alloy via selective electron beam melting. *Scr. Mater.* 143, 117–121.
- Tan, E.Z.E., Pang, J.H.L., Kaminshi, J., Pepin, H., 2019. Characterisation of porosity, density, and microstructure of directed energy deposited stainless steel AISI 316L. *Addit. Manuf.* 25, 286–296.

- Taniguchi, N., Fujibayashi, S., Takemoto, M., Sasaki, K., Otsuki, B., Nakamura, T., Matsushita, T., Kokubo, T., Matsuda, S., 2016. Effect of pore size on bone ingrowth into porous titanium implants fabricated by additive manufacturing: an in vivo experiment. *Mater. Sci. Eng. C* 59, 690–701.
- Terrazas, C.A., Gaytan, S.M., Rodriguez, E., Espalin, D., Murr, L.E., Medina, F., Wicker, R.B., 2014. Multi-material metallic structure fabrication using electron beam melting. *Int. J. Adv. Manuf. Technol.* 71, 33–45.
- Thijs, L., Verhaeghe, F., Craeghs, T., Van Humbeeck, J., Kruth, J.P., 2010. A study of the microstructural evolution during selective laser melting of Ti-6Al-4V. *Acta Mater.* 58, 3303–3312.
- Tolochko, N.K., Savich, V.V., Laoui, T., Froyen, L., Onofrio, G., Signorelli, E., Titov, V.I., 2002. Dental root implants produced by the combined selective laser sintering/melting of titanium powders. *Proc. Inst. Mech. Eng. L J. Mater. Des. Appl.* 216, 267–270.
- Tolosa, I., Garcandía, F., Zubiri, F., Zapirain, F., Esnaola, A., 2010. Study of mechanical properties of AISI 316 stainless steel processed by “selective laser melting”, following different manufacturing strategies. *Int. J. Adv. Manuf. Technol.* 51, 639–647.
- Traini, T., Mangano, C., Sammons, R.L., Mangano, F., Macchi, A., Piattelli, A., 2008. Direct laser metal sintering as a new approach to fabrication of an isoelastic functionally graded material for manufacture of porous titanium dental implants. *Dent. Mater.* 24, 1525–1533.
- Vamsi Krishna, B., Xue, W., Bose, S., Bandyopadhyay, A., 2008. Functionally graded Co–Cr–Mo coating on Ti–6Al–4V alloy structures. *Acta Biomater.* 4, 697–706.
- Van Bael, S., Chai, Y.C., Truscello, S., Moesen, M., Kerckhofs, G., Van Oosterwyck, H., Kruth, J.P., Schrooten, J., 2012. The effect of pore geometry on the in vitro biological behavior of human periosteum-derived cells seeded on selective laser-melted Ti6Al4V bone scaffolds. *Acta Biomater.* 8, 2824–2834.
- Van der Stok, J., Van der Jagt Olav, P., Amin Yavari, S., De Haas Mirthe, F.P., Waarsing Jan, H., Jahr, H., Van Lieshout Esther, M.M., Patka, P., Verhaar Jan, A.N., Zadpoor Amir, A., Weinans, H., 2012. Selective laser melting-produced porous titanium scaffolds regenerate bone in critical size cortical bone defects. *J. Orthop. Res.* 31, 792–799.
- Vandenbroucke, B., Kruth, J.P., 2007. Selective laser melting of biocompatible metals for rapid manufacturing of medical parts. *Rapid Prototyp. J.* 13, 196–203.
- Venugopal, S., Vasudevan, M., Venugopal, S., Sivaprasad, P.V., Jha, S.K., Pandey, P., Mannan, S.L., Prasad, Y.V.R.K., 1996. Industrial validation of processing maps of 316L stainless steel using hot forging, rolling and extrusion. *Mater. Sci. Technol.* 12, 955–962.
- Wang, B.L., Mai, Y.W., Noda, N., 2002. Fracture mechanics analysis model for functionally graded materials with arbitrarily distributed properties. *Int. J. Fract.* 116, 161–177.
- Wang, C., Tan, X., Liu, E., Tor, S.B., 2018. Process parameter optimization and mechanical properties for additively manufactured stainless steel 316L parts by selective electron beam melting. *Mater. Des.* 147, 157–166.
- Wang, L., Xue, J., Wang, Q., 2019. Correlation between arc mode, microstructure, and mechanical properties during wire arc additive manufacturing of 316L stainless ste. *Mater. Sci. Eng. A* 751, 183–190.
- Warnke, P.H., Douglas, T., Wollny, P., Sherry, E., Steiner, M., Galonska, S., Becker, S.T., Springer, I.N., Wiltfang, J., Sivananthan, S., 2008. Rapid prototyping: porous titanium alloy scaffolds produced by selective laser melting for bone tissue engineering. *Tissue Eng. Part C Methods* 15, 115–124.
- Watari, F., Yokoyama, A., Saso, F., Uo, M., Kawasaki, T., 1996. Fabrication and properties of functionally graded dental implant. *Compos. Part B* 28, 5–11.

- Watari, F., Yokoyama, A., Omori, M., Hirai, T., Kondo, H., Uo, M., Kawasaki, T., 2004. Biocompatibility of materials and development to functionally graded implant for bio-medical application. *Compos. Sci. Technol.* 64, 893–908.
- Wauthle, R., Vrancken, B., Beynaerts, B., Jorissen, K., Schrooten, J., Kruth, J.P., Van Humbeeck, J., 2015. Effects of build orientation and heat treatment on the microstructure and mechanical properties of selective laser melted Ti6Al4V lattice structures. *Addit. Manuf.* 5, 77–84.
- Wehmoller, M., Warnke, P.H., Zilian, C., Eufinger, H., 2005. Implant design and production – a new approach by selective laser melting. In: Lemke, H.U., Inamura, K., Doi, K., Vannier, M.W., Farman, A.G. (Eds.), *CARS 2005: Computer Assisted Radiology and Surgery*. Elsevier Science Bv, Amsterdam, pp. 690–695.
- Wei, Z.J., Cao, L., Wang, H.W., Zou, C.M., 2011. Microstructure and mechanical properties of TiC/Ti–6Al–4V composites processed by in situ casting route. *Mater. Sci. Technol.* 27, 1321–1327.
- Wei, C., Li, L., Zhang, X., Chueh, Y.-H., 2018. 3D printing of multiple metallic materials via modified selective laser melting. *CIRP Ann.* 67 (1), 245–248.
- Weinmann, M., Schnitter, C., Stenzel, M., Markhoff, J., Schulze, C., Bader, R., 2018. Development of bio-compatible refractory Ti/Nb(/Ta) alloys for application in patient-specific orthopaedic implants. *Int. J. Refract. Met. Hard Mater.* 75, 126–136.
- Wen, P., Jauer, L., Voshage, M., Chen, Y., Poprawe, R., Schleifenbaum, J.H., 2018a. Densification behavior of pure Zn metal parts produced by selective laser melting for manufacturing biodegradable implants. *J. Mater. Process. Technol.* 258, 128–137.
- Wen, P., Voshage, M., Jauer, L., Chen, Y., Qin, Y., Poprawe, R., Schleifenbaum, J.H., 2018b. Laser additive manufacturing of Zn metal parts for biodegradable applications: processing, formation quality and mechanical properties. *Mater. Des.* 155, 36–45.
- Weng, F., Chen, C., Yu, H., 2014. Research status of laser cladding on titanium and its alloys: a review. *Mater. Des.* 58, 412–425.
- Wiria, F.E., Leong, K.F., Chua, C.K., Liu, Y., 2007. Poly-ε-caprolactone/hydroxyapatite for tissue engineering scaffold fabrication via selective laser sintering. *Acta Biomater.* 3, 1–12.
- Witte, F., Hort, N., Vogt, C., Cohen, S., Kainer, K.U., Willumeit, R., Feyerabend, F., 2008. Degradable biomaterials based on magnesium corrosion. *Curr. Opin. Solid State Mater. Sci.* 12, 63–72.
- Wu, S.H., Li, Y., Zhang, Y.Q., Li, X.K., Yuan, C.F., Hao, Y.L., Zhang, Z.Y., Guo, Z., 2013a. Porous titanium-6 aluminum-4 vanadium cage has better osseointegration and less micromotion than a poly-ether-ether-ketone cage in sheep vertebral fusion. *Artif. Organs* 37, E191–E201.
- Wu, L., Zhu, H., Gai, X., Wang, Y., 2013b. Evaluation of the mechanical properties and porcelain bond strength of cobalt-chromium dental alloy fabricated by selective laser melting. *J. Prosthet. Dent.* 111, 51–55.
- Xia, M., Liu, A., Hou, Z., Li, N., Chen, Z., Ding, H., 2017. Microstructure growth behavior and its evolution mechanism during laser additive manufacture of in-situ reinforced (TiB+TiC)/Ti composite. *J. Alloys Compd.* 728, 436–444.
- Xiao, Z., Yang, Y., Xiao, R., Bai, Y., Song, C., Wang, D., 2018. Evaluation of topology-optimized lattice structures manufactured via selective laser melting. *Mater. Des.* 143, 27–37.
- Xin, X.Z., Chen, J., Xiang, N., Wei, B., 2013. Surface properties and corrosion behavior of Co-Cr alloy fabricated with selective laser melting technique. *Cell Biochem. Biophys.* 67, 983–990.
- Xue, Y., Wang, H.M., 2005. Microstructure and wear properties of laser clad TiCo/Ti2Co intermetallic coatings on titanium alloy. *Appl. Surf. Sci.* 243, 278–286.

- Yadollahi, A., Shamsaei, N., Thompson, S.M., Seely, D.W., 2015. Effects of process time interval and heat treatment on the mechanical and microstructural properties of direct laser deposited 316L stainless steel. *Mater. Sci. Eng. A* 644, 171–183.
- Yan, C., Hao, L., Hussein, A., Young, P., Raymont, D., 2014a. Advanced lightweight 316L stainless steel cellular lattice structures fabricated via selective laser melting. *Mater. Des.* 55, 533–541.
- Yan, C., Hao, L., Hussein, A., Bubb, S.L., Young, P., Raymont, D., 2014b. Evaluation of lightweight AlSi10Mg periodic cellular lattice structures fabricated via direct metal laser sintering. *J. Mater. Process. Technol.* 214, 856–864.
- Yan, W., Ge, W., Smith, J., Lin, S., Kafka, O.L., Lin, F., Liu, W.K., 2016. Multi-scale modeling of electron beam melting of functionally graded materials. *Acta Mater.* 115, 403–412.
- Yang, S., Evans, J.R.G., 2004. A multi-component powder dispensing system for three dimensional functional gradients. *Mater. Sci. Eng. A* 379, 351–359.
- Yang, S.F., Leong, K.F., Du, Z.H., Chua, C.K., 2002. The design of scaffolds for use in tissue engineering. Part II. Rapid prototyping techniques. *Tissue Eng.* 8, 1–11.
- Yang, Y.Q., Lu, J.B., Luo, Z.Y., Wang, D., 2012. Accuracy and density optimization in directly fabricating customized orthodontic production by selective laser melting. *Rapid Prototyp. J.* 18, 482–489.
- Yasa, E., Deckers, J., Kruth, J.-P., 2011. The investigation of the influence of laser re-melting on density, surface quality and microstructure of selective laser melting parts. *Rapid Prototyp. J.* 17, 312–327.
- Yeong, W.Y., Chua, C.K., Leong, K.F., Chandrasekaran, M., 2004. Rapid prototyping in tissue engineering: challenges and potential. *Trends Biotechnol.* 22, 643–652.
- Yeong, W.Y., Sudarmadji, N., Yu, H.Y., Chua, C.K., Leong, K.F., Venkatraman, S.S., Boey, Y.C.F., Tan, L.P., 2009. Porous polycaprolactone scaffold for cardiac tissue engineering fabricated by selective laser sintering. *Acta Biomater.* 6, 2028–2034.
- Yusuf, S.M., Gao, N., 2017. Influence of energy density on metallurgy and properties in metal additive manufacturing. *Mater. Sci. Technol.* 33, 1269–1289.
- Zhang, L., Wang, J., 2014. Effect of temperature and loading mode on environmentally assisted crack growth of a forged 316L SS in oxygenated high-temperature water. *Corros. Sci.* 87, 278–287.
- Zhang, L.C., Klemm, D., Eckert, J., Hao, Y.L., Sercombe, T.B., 2011. Manufacture by selective laser melting and mechanical behavior of a biomedical Ti-24Nb-4Zr-8Sn alloy. *Scr. Mater.* 65, 21–24.
- Zhao, C., Fezzaa, K., Cunningham, R.W., Wen, H., Carlo, F., Chen, L., Rollett, A.D., Sun, T., 2017. Real-time monitoring of laser powder bed fusion process using high-speed X-ray imaging and diffraction. *Sci. Rep.* 7, 3602.
- Zhong, Y., Rannar, L.-E., Liu, L., Koptuyg, A., Wikman, S., Olsen, J., Cui, D., Shen, Z., 2017. Additive manufacturing of 316L stainless steel by electron beam melting for nuclear fusion applications. *J. Nucl. Mater.* 486, 234–245.
- Zhou, L., Yuan, T., Li, R., Tang, J., Wang, M., Mei, F., 2018a. Anisotropic mechanical behavior of biomedical Ti-13Nb-13Zr alloy manufactured by selective laser melting. *J. Alloys Compd.* 762, 289–300.
- Zhou, L., Yuan, T., Li, R., Tang, J., Wang, M., Mei, F., 2018b. Microstructure and mechanical properties of selective laser melted biomaterial Ti-13Nb-13Zr compared to hot-forging. *Mater. Sci. Eng. A* 725, 329–340.